Appl Phys B (2008) 93: 531–538
DOI 10.1007/s00340-008-3217-x

Applied Physics B
Lasers and Optics

Nonlinear refractive index of multicomponent glasses designed for fabrication of photonic crystal fibers

D. Lorenc · M. Aranyosiova · R. Buczynski · R. Stepien · I. Bugar · A. Vincze · D. Velic

Received: 23 April 2008 / Revised version: 13 August 2008 / Published online: 3 October 2008

Abstract The second order nonlinear refractive index n_2 of various multicomponent glasses was measured at the wavelength of 1240 nm close to the 1.3-μm fiber transmission window. With the refractive index covering the range from 1.45 to 2.3, a comparatively broad range of n_2 with values from 1.1×10^{-20} m^2/W for boro-silicate based glass NC21 to 4.3×10^{-19} m^2/W for lead–bismuth-gallate based glass PBG08 was measured using the Z-scan method. Considering the broad infrared transmission range of multicomponent glasses, these materials pose a great potential for future applications as photonic crystal fiber sources of infrared supercontinuum.

PACS 42.65.Jx · 42.70.Ce

1 Introduction

Nonlinear effects are known to have a great impact on ultrashort laser phenomena. Besides harmonic generation and various parametric processes, there is also growing interest in third-order effects of nonlinear refraction and absorption. Moreover, the introduction of photonic crystal fibers (PCFs) [1] resulted in a revival of the research on nonlinear spectral transformations both experimentally and theoretically. With one of the most appealing goals being the generation of broadband supercontinuum [2, 3], an accurate knowledge of the nonlinear Kerr coefficient n_2 [4] is of great value. The material of choice for the PCF fabrication was and still remains silica glass mostly through its availability and good optical performance in the visible/near infrared (VIS/NIR). As a result, most of the previous work on PCFs has been performed using ordinary silica glass. Only recently [5] have multicomponent glasses entered the domain of PCFs. Since the melting point of composite glass is lower than that of fused silica, complex and nontrivial air–glass structures became accessible. Multicomponent glasses provide both higher refractive indices at comparable wavelengths and enhanced Kerr nonlinearity. Most notably, because of their broad transmission range covering the NIR, they are envisioned as suitable sources of IR supercontinuum [6–8]. Indeed, one of the most recent works [9] demonstrated supercontinuum with a bandwidth of over 4000 nm spanning the IR from 789 nm to almost 5 μm.

Several approaches suitable for measurement of refractive nonlinearity have been proposed, among them nonlinear interferometry [10, 11], degenerate and nearly degenerate three-wave mixing (TWM) [12], ellipse rotation [13] and beam distortion measurements [14], though the Z-scan technique is probably the most frequently employed one. Since its first announcement [15], a broad range of media which exhibit nonlinear refraction and/or multiphonon absorption became the subject of investigation. Besides the high sensitivity of the Z-scan method comparable to inter-

D. Lorenc (✉) · M. Aranyosiova · I. Bugar · A. Vincze · D. Velic
International Laser Centre, Ilkovicova 3, 841 04 Bratislava, Slovakia
e-mail: lorenc@ilc.sk

M. Aranyosiova · D. Velic
Department of Physical and Theoretical Chemistry, Faculty of Natural Sciences, Comenius University, 842 15 Bratislava, Slovakia

R. Buczynski
Information Optics Group, Faculty of Physics, Warsaw University, Pasteura 7, 02-093 Warsaw, Poland

R. Stepien
Institute of Electronic Materials Technology, Wólczyńska 133, 01-919 Warsaw, Poland

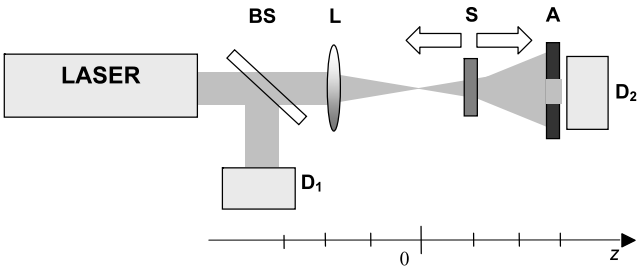

Fig. 1 The basic arrangement of a Z-scan experiment. BS—beam splitter, L—lens, S—sample, A—pinhole, D_1, D_2—detectors

ferometric techniques, there is also the advantage of obtaining not only the value but also the sign of the third-order susceptibility of a material. The technique allows us to separately determine the real and imaginary parts of the third-order susceptibility, which result from Kerr nonlinearity and two-photon absorption (TPA), respectively. Among the materials that have been successfully studied, there is a broad range of semiconductors [16–19] and wide-gap solids [20], all showing a reasonable agreement with theory.

In this work, we report an experimental investigation of refractive nonlinearity in novel multicomponent glass samples designated specifically for the fabrication of PCFs. A subnanosecond laser source employed for the study was derived from an amplified femtosecond Cr:Forsterite laser system providing pulses with the wavelength of 1240 nm. Since the nonlinear refractive index is wavelength dependent, a laser source with an output wavelength in the close proximity to the 1.3-μm fiber transmission window is of great value. It is shown that for sufficiently high values of input irradiance, the self-phase modulation might have a detrimental effect on the measured values of the nonlinear refractive index.

2 Theory

The experimental study was performed using the sensitive transmission Z-scan method [15] (Fig. 1), which is similar to photothermal (thermal lens) spectroscopy [21]. The sample is moved axially (along the z-axis) in the region near the beam waist and the transmittance of the nonlinear medium (sample) through a finite aperture in the far field is measured as a function of sample position with respect to the beam waist. Instead of phase changes being introduced by the dependence of refractive index upon sample temperature $n(T)$ as in the case of thermal lens spectroscopy, the incident radiation may alter the refractive index of a nonlinear medium through a 'third-order' dependence $n(I)$.

Supposing a TEM_{00} Gaussian beam and following the procedure given by Sheik-Bahae et al. [22], the normalized transmittance is obtained as

$$T(z) = \frac{\int_{-\infty}^{\infty} P_{\mathrm{T}}(\Delta\phi_0(t))\,\mathrm{d}t}{S\int_{-\infty}^{\infty} P_{\mathrm{i}}(t)\,\mathrm{d}t}, \tag{1}$$

where $P_{\mathrm{i}}(t) = \pi w_0^2 I_0(t)/2$ is the instantaneous input power (corrected for reflection from the sample surface), w_0 being the beam waist radius, $S = 1 - \exp(-2r_{\mathrm{a}}^2/w_{\mathrm{a}}^2)$ is the aperture linear transmittance with w_{a} being the beam radius in the aperture plane and r_{a} being the aperture radius, P_{T} is the power transmitted through the aperture in the Z-scan regime and $\Delta\phi_0(t)$ are the on-axis phase changes. Note that $T(z)$ is to be considered as the quantity measured experimentally when performing a Z-scan experiment. It was shown [22] that in the limit of small nonlinear phase change ($|\Delta\phi_0| \ll 1$), the expression (1) may be approximated by

$$T(z, \Delta\phi_0) = 1 - \frac{4\Delta\phi_0 x}{(x^2+9)(x^2+1)}, \tag{2}$$

where $x = z/z_0$ and z_0 is the Rayleigh distance, which is the approach used mostly throughout this paper. On the other hand for larger phase distortions ($|\Delta\phi_0| > 1$) the symmetry of the Z-scan curves (see e.g. [22]) is broken, but nevertheless the following expressions still apply:

$$\begin{aligned} \Delta Z_{\mathrm{p-v}} &= 1.7 z_0, \\ \Delta T_{\mathrm{p-v}} &\cong 0.406(1-S)^{0.25}|\Delta\phi_0|. \end{aligned} \tag{3}$$

For a small (pinhole) aperture $S \to 0$ and consequently:

$$\Delta T_{\mathrm{p-v}} \cong 0.406|\Delta\phi_0|, \tag{4}$$

where ΔT_{p-v} is the difference between the normalized peak and valley transmittances, ΔZ_{p-v} is the spatial separation between peak and valley and $|\Delta\phi_0|$ is the on-axis phase shift at the focus.

Using the Z-scan technique, both the nonlinear refractive index n_2 and the nonlinear absorption coefficient β may be obtained simultaneously. As has been shown [22], when the aperture is removed as for the open-aperture Z-scan, detection is no longer sensitive to phase changes introduced by the sample through eliminated spatial resolution in the detection plane. Thus, only the influence of nonlinear absorption has to be considered. On the other hand, the closed-aperture Z-scan in the case of media showing both refractive and absorptive nonlinearities is sensitive to both the nonlinear refraction and the nonlinear absorption. Thus, performing the closed-aperture Z-scan measurement followed by the open-aperture one, both n_2 and β are determined.

The thin-sample approach was used throughout the theoretical analysis. A sample is considered to be thin if $d < n_0 z_0$, where d is the sample physical thickness and z_0 is the

confocal (Rayleigh) distance [22]. Moreover, for ultra short (<1 ps) pulses, the increase of pulse width inside the sample due to group velocity dispersion (GVD) [23] must be considered. Pulse broadening may alter the peak irradiance and hence the magnitude of the nonlinear phase shift inside the sample. The pulse duration effect was expressed in terms of the dispersion distance L_D, defined as the length over which a transform-limited Gaussian pulse broadens by a factor of $\sqrt{2}$ due to the second-order dispersion [4]:

$$L_D = \frac{T_0^2}{|\beta_2|}, \tag{5}$$

where T_0 is the pulse duration and β_2 is the GVD parameter. When the sample length exceeds the value of L_D, the pulse broadening becomes significant. The dispersion distances must be calculated separately for each material using appropriate Sellmeier equations. In the high-intensity regime, i.e. for high peak power, even the pulse broadening induced by self-phase modulation (SPM) can play a significant role in altering the peak irradiance in a way similar to the case of GVD. As in the previous case, the nonlinear distance L_{NL} is defined as [4]

$$L_{NL} = \frac{1}{\gamma P_0}, \tag{6}$$

where γ is the nonlinear parameter [4] and P_0 is the peak power. If the sample width $d > L_{NL}$, SPM will have a detrimental effect on the Z-scan measurements.

The second order nonlinear refractive index, the Kerr index and the nonlinear absorption coefficient all exhibit the dispersion dependence. Moreover, the dispersion dependence of the linear refractive index near the absorption edge behaves similarly to the dispersion of nonlinear refraction near the two-photon absorption (2PA) edge. Following this analogy, a nonlinear equivalent to the Kramers–Krönig relation was previously used to obtain the appropriate dispersion equation [24]:

$$n_2 = K' \frac{\sqrt{E_p}}{n_0 E_g^4} G_2(\hbar\omega/E_g) \quad \text{[esu]}, \tag{7}$$

where K' is a material-independent constant with a value of 7.33×10^{-9} [20] calculated from the two-band parabolic approximation, E_p is the Kane momentum related parameter with a value of 21 eV for a large number of materials, E_g is the band-gap energy and $G_2(x)$ is a function solely of the ratio between the photon energy and the material energy gap. This model was successfully applied to a broad range of semiconductors [25] and wide-gap solids [20].

Originally Boling, Glass and Owyoung [26] introduced a different empirical expression for n_2:

$$n_2 = \frac{K(n_d - 1)(n_d^2 + 2)^2}{\nu_d(1.517 + \frac{(n_d^2+2)(n_d+1)}{6n_d}\nu_d)^{1/2}} \times 10^{-13} \quad \text{[esu]}, \tag{8}$$

where n_d is the linear refractive index at the d line of He at 587.56 nm and ν_d is the Abbe number defined elsewhere [27]. K is an empirical factor which is supposed to be reasonably constant for a group of related materials. Expression (8) was already shown to be fairly successful in predicting the nonlinear refractive index of glasses [28].

3 Experiment

Initially, an amplified Cr:Forsterite laser system delivering pulses centered at a wavelength of 1240 nm with a repetition rate of 50 Hz and a pulse duration of 110 fs was employed as the pump source for the Z-scan measurements. The system was designed to support pulse energies of up to 1 mJ per pulse; however, rather low energies ranging from 2 to 10 μJ were employed for the Z-scan experiments. Detector D_1 served as a reference and the signal was sampled as D_2/D_1. Furthermore, a boxcar integrator and averager system was used to collect the preamplified signal from the detector D_2, thus substantially increasing the sensitivity of the experimental setup. Typically, 100 samples were averaged, increasing the signal to noise ratio by a factor of 10. However, even for the modest pulse energy of 2 μJ, the obtained values of n_2 were strongly influenced by the SPM suppression of peak power (6). Subsequent calculations revealed L_{NL} being of the order of 10^{-4} m, i.e. approximately one-tenth of the sample thickness. Under these conditions, the influence of SPM became dominant resulting in n_2 values differing considerably from those given in the literature. Further decrease of the pulse peak power by lowering of pulse energy provided no desirable effect since it resulted in low average power at the detector being under the detection limit of the boxcar scheme. The original setup was therefore modified by omitting the compressor from the CPA (Chirped Pulse Amplification) system thereby increasing the pulse duration by a factor of 10^3, resulting in a value of approximately 185 ps. The actual values of pulse duration were measured by a BIFO K008 streak camera.

Two groups of bulk samples were used. The multicomponent, composite glass samples SK 222, NC 21A, PBG1, PBG08 and TWNB were produced, cut and polished at the Institute of Electronic Materials Technology (ITME) in Warsaw. The SK2 sample was produced commercially and used along with F2 and SF57 as references in order to compare the obtained results to the published data. Chemical compositions of the bulk multicomponent glass samples are given in Table 1. Thermomechanical properties of the samples prepared at ITME are summarized in Table 2. Note that all glasses made at ITME are tested against crystallization during thermal/mechanical processing of drawing, i.e. all considered glasses are resistant for devitrification during

Table 1 Chemical composition of the bulk multicomponent glass samples

Glass designation	Composition
NC21A	55% SiO_2, 1% Al_2O_3, 26% B_2O_3, 3% Li_2O, 9.5% Na_2O, 5.5% K_2O, 0.8% As_2O_3
SK222	68.4% SiO_2, 2.4% Al_2O_3, 2% B_2O_3, 12.3% Na_2O, 0.7% K_2O
F2	45.7% SiO_2, 45.5% PbO, 3.5% Na_2O, 5.0% K_2O, 0.8% As_2O_3, commercial
SF57	PbO–SiO_2, commercial
PBG1	56.70% SiO_2, 0.35% Al_2O_3, 30.00% PbO, 4.15% Na_2O, 8.65% K_2O
PBG08	14.06% SiO_2, 39.17% PbO, 27.26% Bi_2O_3, 14.26% Ga_2O_3, 5.26% CdO
TWNB	70–80 %mol TeO_2, 10–20% mol ZnO, 10–15 %mol K_2O/Na_2O
SK2	SiO_2–B_2O_3–BaO, commercial

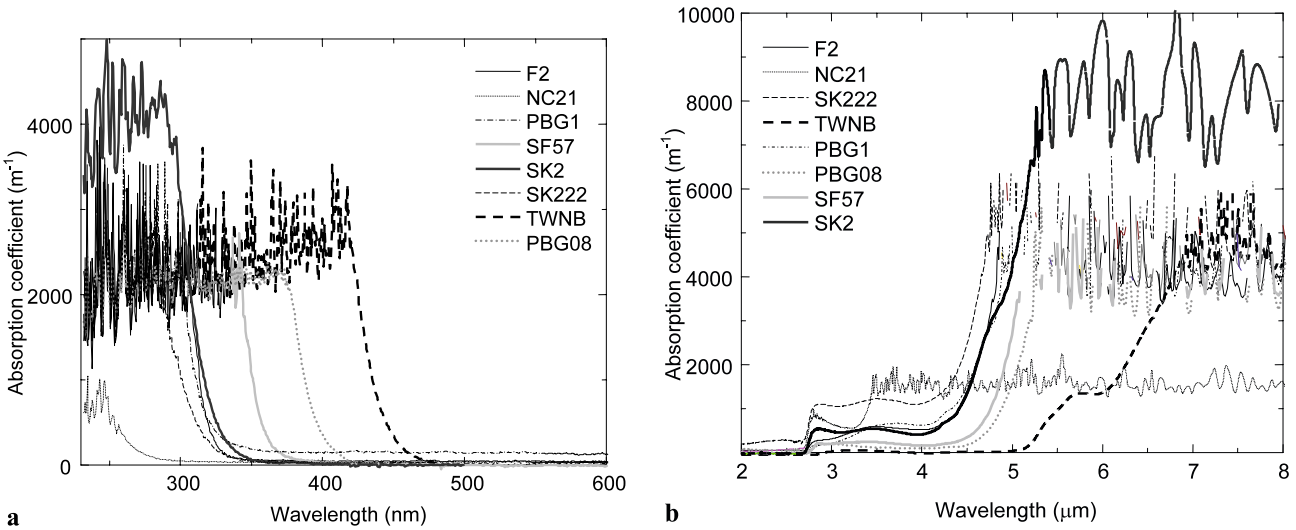

Fig. 2 The UV absorption cutoffs of multicomponent samples (**a**) and corresponding multiphonon (IR) absorption edges (**b**)

fiber drawing and no crystal nuclei are observed in the samples under electron and/or optical microscopes. The glasses are therefore suitable for fabrication of PCFs and the obtained fibers are mechanically resistant. An actual example of a PCF made of the SK222 prepared at ITME can be found elsewhere [29].

4 Results and discussion

In general, composite glasses with a composition such as given in Table 1 were expected to exhibit higher refractive indices and up to one order of magnitude higher nonlinearity than fused silica. Previously, the considered multicomponent glasses were shown to have the multiphonon IR absorption edge substantially shifted into the IR [30] making them an ideal choice for NIR applications. The absorption measurements for the samples are shown Fig. 2. Notably SK2, SK222, F2 and PBG1 all show very similar ultraviolet (UV) transmission cutoffs implying some similarities as will be described in greater detail in this section. On the other hand, the light NC21 glass and the heavy tellurite TWNB glass are on the very margins of the spectra as is also confirmed by the absorption measurements in the IR shown in Fig. 2b. The PBG08, SF57 and TWNB glasses all show improved IR performance as compared to silica with the tellurite glass TWNB being highly transparent up to the 5.2-μm wavelength.

In order to extract a correct value of n_2 using the above-described Z-scan technique, all input irradiances were corrected for Fresnel reflection losses and therefore the real refractive index n had to be known. The corresponding dispersion of the linear refractive index is shown in Fig. 3a. The dispersion curves for reference samples SF57, F2 and SK2 were extracted using the appropriate Sellmeier coefficients [31]. For the NC21 and SK222 glasses developed at ITME, first a prism was cut and polished out of the bulk glass and the refractive index was measured in the VIS from 0.4 to 0.7 μm. The measured data were then fitted and extrapolated up to the wavelength of 2 μm using the Sellmeier formula in the form

Table 2 Thermomechanical properties of the samples prepared at ITME

Glass type	SK222	PBG1	NC21A	TWNB	PBG08
α [10^{-7} K^{-1}]*	84.0	94.0	87.5	158.2	81.5
Glass transition temperature T_g [°C]	542	427	492	356	470
Dilatometric softening point T_d [°C]	610	468	545	370	500
Melting temperature T_m [°C]	1480	1350	1280	800	1100
Purity of raw materials	Pure; tech. purity	Pure; tech. purity	Pure per analyse	99.9%	99.9%
Duration of melting [h]	24	24	6	1	5.5
Type of crucible	Glass melting tank	Glass melting tank	Platinum	Gold	Platinum
Homogeneity of sample	Very high	Very high	Very high	High	High
Sample dimensions [mm × mm × mm]	10 × 10 × 1.80	10 × 10 × 1.85	9 ×9 × 5.14	10 × 10 × 1.90	10 × 10 × 2.00

*Linear coefficient of thermal expansion in the range of temperature 20–300°C

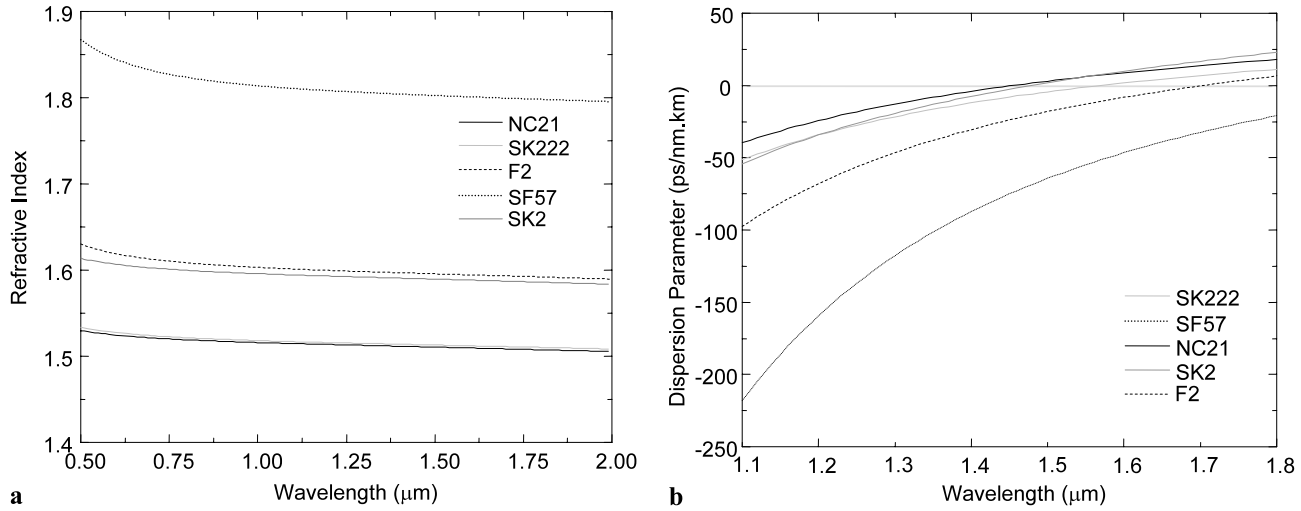

Fig. 3 Calculated dispersion of linear refractive index (**a**) and corresponding dispersion coefficient for the given multicomponent glass samples (**b**)

$$n^2 = 1 + \frac{K_1\lambda^2}{\lambda^2 - L_1} + \frac{K_2\lambda^2}{\lambda^2 - L_2} + \frac{K_3\lambda^2}{\lambda^2 - L_3}, \tag{9}$$

where λ is the wavelength and K_i, L_i are the material-specific coefficients. Finally, only refractive-index values at the discrete wavelength of 589.3 nm were known for PBG1, PBG08 and TWNB glasses at the time of this study. Their values for the applied wavelength of 1240 nm have been extrapolated using dispersion dependences for the well-known glasses with similar composition [31]. Such a procedure is justified because apart from the Fresnel losses the Z-scan method is virtually independent of the refractive index, meaning that the impact of n is rather low. In order to estimate the influence of the GVD on the pulse broadening, the dispersion parameter [4] was calculated using the dispersion curves given in Fig. 3a. As shown in Fig. 3b, rather low dispersion parameters at 1240 nm ranging from −19 ps/nm km for NC21 to −141 ps/nm km for SF57 are observed giving the corresponding dispersion lengths between 8×10^5 and 1×10^5 m, respectively. Obviously, the GVD influence on the pulse broadening and peak power is negligible under these conditions and the pulse evolution is dominated by the SPM-induced broadening. After the initial femtosecond experimental scheme was modified by omitting the compressor from the amplifier as described in Sect. 3, nonlinear lengths of several 10^{-2} m were obtained, i.e. approximately one order of magnitude larger than the sample thickness (see Table 1 for comparison). Consequently, an experimental regime was accessed where the Z-scans are virtually free of the influence of both the GVD and SPM effects.

Since the theoretical model for n_2 (7) depends upon the fourth power of E_g, the band-gap energy had to be known

Table 3 Band-gap energy of the multicomponent glass samples calculated using the Tauc-plot procedure along with the thickness and refractive index at the wavelength of 1240 nm

Glass designation	Thickness [mm]	E_g [eV]	n_{1240nm}
NC21A	5.14	4.21	1.51
SK222	1.80	3.67	1.52
F2	2.00	3.76	1.60
SF57	2.00	3.34	1.81
PBG1	1.85	3.78	1.56
PBG08	2.00	3.02	2.30
TWNB	1.90	2.69	2.22
SK2	1.01	3.65	1.59

with high precision. The band-gap energy was extracted using the *Tauc-plot* procedure [32]. Briefly, under the assumption of a direct transition, the term $(\alpha h\nu)^{0.5}$, with α being the linear absorption coefficient and $h\nu$ being the photon energy is plotted versus the photon energy. Consequently, a linear *Tauc region* appears just above the optical absorption edge and the extrapolation of this line to the photon energy axis yields the band-gap energy. The Tauc-plot procedure was successfully applied to the multicomponent glass samples under study and the results are shown in Table 3.

Individual Z-scans are presented in Fig. 4. In order to avoid the damage of the sample, different incident pulse energies had to be used in individual cases. Most notably for PBG08 the highest applicable pulse energy was limited to approximately 50 μJ for a pulse length of 185 ps FWHM. In general, the materials are assumed to become two-photon absorbing when the photon energy $h\nu$ equals one-half of the band-gap energy E_g [20]. Since at the wavelength of 1240 nm the photon energy ∼1 eV and the lowest band-gap energy was shown to be 2.69 eV (TWNB glass, see Table 3 for comparison), no two-photon absorption was expected in our case. Indeed no traces of the two-photon absorption (2PA) effects were observed as is also confirmed by the symmetry of the curves given in Fig. 4. Note that the horizontal shift of the Z-scan curves in Fig. 4 was caused by the change of sample position between successive measurements and not by an inherent nature of the experiment. Because of a small phase change in the upper six cases in Fig. 4, the simple analytical expression (2) was employed to fit the data. However, because of high Kerr nonlinearity of TWNB and PBG08, the imposed phase change in both of these cases was significant and the data could not be fitted with the analytical model. Therefore, the appropriate analysis for larger phase distortions had to be performed ((3) and (4)). Great care was taken in preserving the linear response of the detector and hence the diameter of the pinhole was chosen to be much smaller than the beam diameter

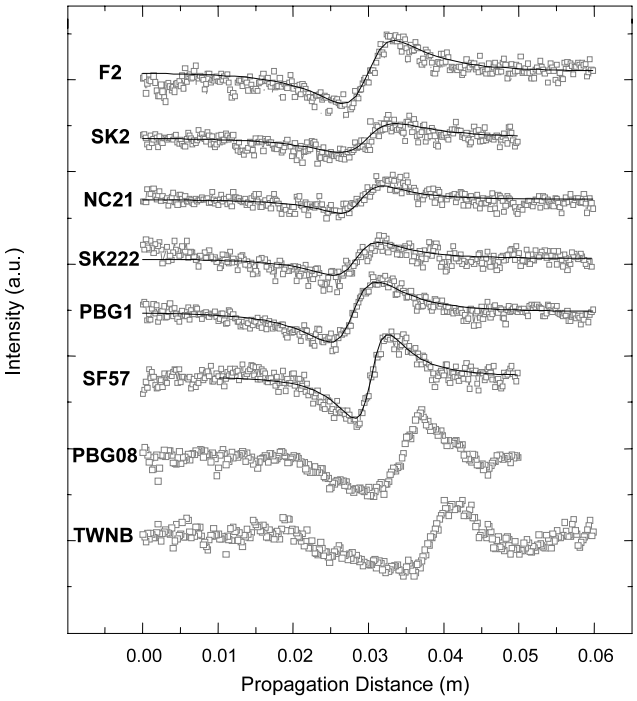

Fig. 4 Measured Z-scan traces along with the calculated fitting curves. Because of the large phase distortions imposed in the cases of PBG08 and TWNB, n_2 was evaluated using a numerical approach (4)

in the detection plane ($S \sim 0.0026$). Consequently, the approximate model (4) was applied instead of the more general form (3). Indeed, for such a low value of S the actual difference between solutions of (3) and (4) is less than 1%. The obtained values of the nonlinear refractive index n_2 are summarized in Table 4. Note that all values of input irradiance used in the calculation of n_2 were corrected for Fresnel reflection losses using the appropriate refractive-index values given in Table 3. As was noted in earlier work [33], the error analysis in Z-scan-type experiments is not straightforward. In agreement with previous work [22], we conclude that the error of the obtained values was ±30%, being induced mainly by the uncertainty of the measured incident energy. Also, it is valuable to note that the values of n_2 for glasses given in the reference books (see e.g. [27]) usually differ from each other considerably even for similar experimental conditions.

The two-parabolic-band model (7) was initially applied in order to obtain the theoretical values of n_2. However, the introduction of band-gap energies obtained by the Tauc-plot procedure and given in Table 3 into expression (7) yielded unrealistically high values of n_2 ranging from 3.3×10^{-19} m^2/W for the NC21 sample to 1.2×10^{-18} m^2/W for TWNB. Apparently, the two-parabolic-band model systematically overestimated the value of n_2. As was confirmed by previous work [20], the model was quite successful in predicting the n_2 values for wide band gap solids but its applicability to low band gap glasses remains questionable. Con-

Table 4 Measured and calculated values of n_2

Glass designation	n_2 (measured) 10^{-20} m^2/W	n_2 (calculated) 10^{-20} m^2/W
NC21	1.1	1.1
SK222	1.6	1.3
F2	2.9	3.0
SF57	13	7.1
PBG1	2.5	2.0
TWNB	18	19
SK2	2.1	1.5
PBG08	43	24

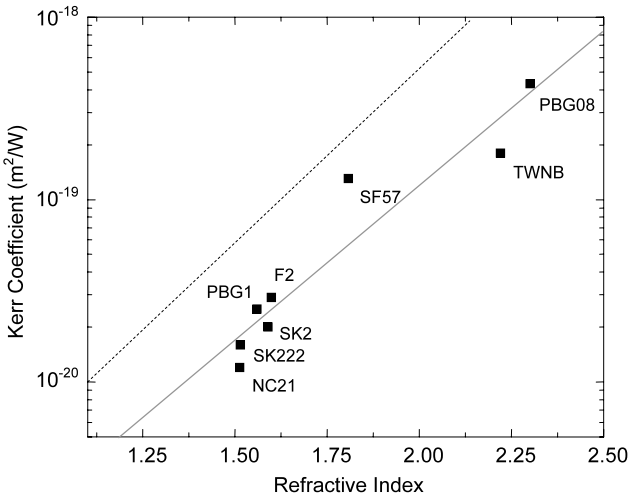

Fig. 5 Relation between the linear and nonlinear refractive indices. The *solid line* is a linear fit of the experimental data and the *dashed line* is a linear fit [7] valid for a broader range of glasses

sequently, the Boling, Glass and Owyoung (BGO) model (8) was applied and the obtained values are given in Table 4. For all cases the characteristic constant K was kept at a value of 100. All of the measured values of n_2 show reasonable agreement with theoretically predicted values. In conclusion, the BGO model apparently achieved higher precision for low band gap multicomponent glasses. The main drawback of the BGO approach is its inability to account for the dispersion of the nonlinear refractive index, since the expression (8) is basically wavelength independent. On the other hand, even considering the dispersion of n_2 within the two-parabolic-band model far away from the 2PA absorption edge (with $h\nu/E_g \sim 0.37$ at most) would not provide any significant effect (see e.g. [20] and the plots of the theoretical dispersion function $G_2(x)$ therein).

In order to gain a more complex overview of the different issues involved, the obtained values of n_2 are plotted against the linear refractive index in Fig. 5. The relationship between the nonlinear refractive index n_2 and the linear refractive index n_0 in glass materials is a well-known feature [7, 27]. The dashed line plotted in Fig. 5 is the linear fit (in log scale) to n_2 of various glasses taken from [7] having values of n_2 ranging from 10^{-20} to 10^{-17} m^2/W. Comparing the measured data and the linear fit would suggest that our measurements systematically underestimate the value of n_2. On the other hand, as shown in Table 4, there is a reasonable agreement between the theoretically predicted values of n_2 and the measured ones. The glasses with n_2 within the range of 10^{-20} to 5×10^{-19} m^2/W are best fitted with a shifted line, whereas the original linear fit is valid in the broader range mentioned above. This conclusion is confirmed when only n_2 data between 10^{-20} and 5×10^{-19} m^2/W are considered from the previously published plot [7].

5 Conclusion

The enhanced linear refractive index covering the range from 1.45 up to 2.3 allows manufacturing of PCFs with index contrast higher than that for silica/air, i.e. approximately 0.5. This enhancement provides the corresponding advantage of better light confinement in the core of the fiber. A comparatively broad range of n_2 is covered by multicomponent glasses starting from values lower than that for silica as for NC21 (1.1×10^{-20} m^2/W) and SK 222 (1.6×10^{-20} m^2/W) up to n_2 being one order of magnitude larger as for SF57 (1.3×10^{-19} m^2/W), TWNB (1.8×10^{-19} m^2/W) and PBG08 (4.3×10^{-19} m^2/W). Considering the broad IR transmission range of multicomponent glasses, these materials pose a great potential for future applications as PCF sources of IR supercontinuum.

Acknowledgements The authors D.L., M.A. and D.V. would like to acknowledge the support from APVT-20-029804 and APVV-0491-07, R.B. and R.S. are grateful for the financial support from Ministry of Science Grant Nos. R02 043 02 and N N507 433934 and I.B. is grateful for the support from VEGA 1/0870/08. The personal support of Dusan Chorvat is gratefully appreciated.

References

1. J.C. Knight, T.A. Birks, P.S.J. Russell, D.M. Atkin, Opt. Lett. **21**, 1547 (1996)
2. J.K. Ranka, R.S. Windeler, A.J. Stentz, Opt. Lett. **25**, 25 (2000)
3. J.M. Dudley, G. Genty, S. Coen, Rev. Mod. Phys. **78**, 1135 (2006)
4. G.P. Agrawal, *Nonlinear Fiber Optics* (Academic, San Diego, 2001)
5. T. Monro, Y. West, D. Hewak, B.N. Richardson, Electron. Lett. **36**, 1998 (2000)
6. V.V.R. Kumar, A. George, W. Reeves, J. Knight, P. Russell, F. Omenetto, A. Taylor, Opt. Express **10**, 1520 (2002)
7. J.H.V. Price, T.M. Monro, H. Ebendorff-Heidepriem, F. Poletti, V. Finazzi, J.Y.Y. Leong, P. Petropoulos, J.C. Flanagan, G. Brambilla, X. Feng, D.J. Richardson, Proc. SPIE **6102**, 61020A 2006)

8. V.I. Kalashnikov, E. Sorokin, I.T. Sorokina, Appl. Phys. B **87**, 37 (2007)
9. P. Domachuk, N.A. Wolchover, M. Cronin-Golomb, A. Wnag, A.K. George, C.M.B. Cordeiro, J.C. Knight, F.G. Omenetto, Opt. Express **16**, 7161 (2008)
10. M.J. Weber, D. Milam, W.L. Smith, Opt. Eng. **17**, 463 (1978)
11. M.J. Moran, C.Y. She, R.L. Carman, IEEE J. Quantum Electron. **11**, 259 (1975)
12. R. Adair, L.L. Chase, S.A. Payne, J. Opt. Soc. Am. B **4**, 875 (1987)
13. A. Owyoung, IEEE J. Quantum Electron. **9**, 1064 (1973)
14. W.E. Williams, M.J. Soileau, E.W. Van Stryland, Opt. Commun. **50**, 256 (1984)
15. M. Sheik-Bahae, A.A. Said, E.W. Van Stryland, Opt. Lett. **14**, 955 (1989)
16. A.A. Said, M. Sheik-Bahae, D.J. Hagan, T.H. Wei, J. Wang, J. Young, E.W. Van Stryland, J. Opt. Soc. Am. B **9**, 405 (1992)
17. K. Lee, W. Cho, J. Park, J. Kim, S. Park, U. Kim, Opt. Lett. **19**, 1116 (1994)
18. J. Wang, M. Sheik-Bahae, A.A. Said, D.J. Hagan, E.W. Van Stryland, J. Opt. Soc. Am. B **11**, 1009 (1994)
19. K.Y. Tseng, K.S. Wong, G.K.L. Wong, Opt. Lett. **21**, 180 (1996)
20. R. DeSalvo, A.A. Said, D.J. Hagan, E.W. Van Stryland, M. Sheik-Bahae, IEEE J. Quantum Electron. **32**, 1324 (1996)
21. J.M. Harris, N.J. Dovichi, Anal. Chem. **52**, 695 (1980)
22. M. Sheik-Bahae, A.A. Said, T. Wei, D.J. Hagan, E.W. Van Stryland, IEEE J. Quantum Electron. **26**, 760 (1990)
23. H.P. Li, C.H. Kam, Y.L. Lam, F. Zhou, W. Ji, Appl. Phys. B **70**, 385 (2000)
24. M. Sheik-Bahae, D.C. Hutchings, D.J. Hagan, E.W. Van Stryland, IEEE J. Quantum Electron. **27**, 1296 (1991)
25. M. Sheik-Bahae, D.J. Hagan, E.W. Van Stryland, Phys. Rev. Lett. **65**, 96 (1990)
26. N.L. Boling, A.J. Glass, A. Owyoung, IEEE J. Quantum Electron. **14**, 601 (1978)
27. M.J. Weber, *Handbook of Optical Materials* (CRC, Boca Raton, 2003)
28. D. Milam, M.J. Weber, J. Appl. Phys. **47**, 2497 (1976)
29. A.V. Mitrofanov, Y.M. Linik, R. Buczynski, D. Pysz, D. Lorenc, I. Bugar, A.A. Ivanov, M.V. Alfimov, A.B. Fedotov, A.M. Zheltikov, Opt. Express **14**, 10645 2006)
30. D. Lorenc, I. Bugar, M. Aranyosiova, R. Buczynski, D. Velic, D. Chorvat, Laser Phys. **18**, 270 (2008)
31. ZEMAX Glass Catalog. ZEMAX Development Corporation, Bellevue, WA, 1990–2000
32. J. Tauc, R. Grigorovici, A. Vancu, Phys. Status Solidi **15**, 627 (1966)
33. S.E. Bialkowski, *Photothermal Spectroscopy Methods for Chemical Analysis* (Wiley, New York, 1996)